Construction and Building Materials 509 (2026) 145226

Contents lists available at ScienceDirect

Construction and Building Materials

journal homepage: www.elsevier.com/locate/conbuildmat

Mechanical and microstructure evolution of the Tou-Kung joints under weathering conditions

Kai Wang [a], Danping Hao [a], Miaomiao Zhao [a], Wei Li [a], Yoshioka Hideki [b], Xueting Yang [a], Shanlong Wang [c], Biao Zhou [a,*]

[a] Inner Mongolia Research Institute, China University of Mining and Technology (Beijing), China University of Mining & Technology (Beijing), Ordos 017010, China
[b] Department of Architecture, Faculty of Engineering, University of Tokyo, Tokyo 113-8654, Japan
[c] Ministry of Emergency Management of the People's Republic of China, Beijing 100713, China

ARTICLE INFO

Keywords:
Tou-Kung joints
Mechanical response
Artificial accelerated weathering
Microstructure

ABSTRACT

Historic buildings possess significant cultural, scientific, and aesthetic value, showcasing the accomplishments of past eras. The mechanical response of the Tou-Kung joints changed after several hundred years of natural weathering. In this study, the effect of weathering on the mechanical response of the Tou-Kung joints is investigated. The conventionally treated Tou-Kung joints were weathered by a standard construction material durability test method and a standard weathering method. Through mass loss rate (MLR), colorimetry, thermogravimetric analysis (TGA), vertical loading test and scanning electron microscopy (SEM), it is found that weathering markedly decreases mechanical response, leading to significant pore formation and phase transitions. Specifically, peak load capacity reduced from 11.77 kN to 9.98 kN. Additionally, stiffness degradation ratios ranged from 0.82 to 0.96 during the strengthening phases. These results indicate substantial degradation of structural integrity, providing critical insights for the development of evaluating structural integrity in heritage conservation contexts.

1. Introduction

The preservation of historical timber structures constitutes a global challenge integral to cultural heritage protection [1]. These structural systems, enduring centuries of exposure, undergo continuous deterioration under environmental stressors [2]. Functioning as a hygroscopic anisotropic biomaterial, timber experiences complex physicochemical and micromechanical transformations when exposed to external conditions, ultimately resulting in structural performance degradation [3]. Elucidating the intricate mechanisms underlying this multidimensional deterioration is paramount for developing effective predictive models and establishing conservation strategies. Traditional Chinese Tou-Kung joints, exemplifying intricate mortise and tenon joints, represent a particularly vulnerable component. These critical structural elements bear substantial mechanical loads while simultaneously defining architectural aesthetics. Nevertheless, research elucidating the multiscale degradation pathways for such geometrically complex, stress-concentrated joints remains notably deficient. Current predictive frameworks frequently lack robust correlations between the regression of mechanical properties and their fundamental chemo-microstructural origins. Consequently, accurately assessing the long-term performance and failure risk inherent within environmentally aged heritage timber structures proves challenging.

The Tou-Kung joint is believed to have originated during the Western Zhou Dynasty and was later formalized in the Song Dynasty through the *Yingzao Fashi*, serving as a hallmark element of East Asian timber-framed architecture [4]. Its layered, interlocking components, connected by intricate mortise-and-tenon joints, function both as load-bearing joints without metal fasteners and as aesthetic units that distribute roof loads [5]. This ingenious structural design endowed historical buildings like the Foguang Temple (857 AD) and Pagoda of Fogong Temple (1056 AD) [6] with exceptional seismic resistance. Over time, Tou-Kung joints evolved from primarily load-bearing components to a symbolic indicator of institutional rank and aesthetic sophistication. Nevertheless, its mechanical performance remains highly sensitive to environmental humidity. Humidity affects wood cell structure and moisture transport,

* Correspondence to: School of Emergency Management and Safety Engineering, China University of Mining & Technology (Beijing), No.11 Xueyuan Road, Haidian District, Beijing 100083, China.
E-mail addresses: zhoubiao1088@bme.arch.t.u-tokyo.ac.jp, zhoubiao1088@gmail.com, zhoubiao1088@cumtb.edu.cn (B. Zhou).

https://doi.org/10.1016/j.conbuildmat.2026.145226
Received 1 August 2025; Received in revised form 6 December 2025; Accepted 9 January 2026
Available online 14 January 2026

leading to diminished mechanical properties [7]. Degradation of structural constituents and irreversible hydrogen bonding impact the hygroscopicity and mechanical performance of dried wood [8].

Conservation efforts for Chinese historical timber buildings have constituted a major research focus in recent years [9]. Predominant scholarly inquiry concentrates on isolated examination of timber weathering phenomena. For instance, profilometry and colorimetry characterize mass loss and surface erosion [10–12], while thermal analysis and spectroscopic techniques quantify polymer degradation [13,14]. Additionally, standardized mechanical testing employs simplified specimens [15,16], and research investigates singular environmental factors affecting wood micromechanics [13,17,18]. Artificially accelerated weathering techniques are also applied to bulk timber samples [19–21]. Disaster mitigation for timber structures represents a critical dimension within the broader field of historical building conservation [22]. This significance stems from the increased fragility of weathered timber structures. However, prevalent conservation practices rely heavily on qualitative inspections or oversimplified empirical models [23–25]. These methodologies are incapable of capturing the intricate interactions driving multiscale degradation. Furthermore, the significance of disaster prevention for historical buildings transcends structural integrity, embodying profound cultural value, thereby motivating extensive recent investigation. As shown in Fig. 1, Tou-Kung joints inevitably degrade under environmental exposure, mirroring the susceptibility of all external timber elements [26]. Given that joint failure jeopardizes overall structural stability, defining their unique degradation trajectories is imperative. However, research quantifying the heterogeneous phenomena occurring within timber Tou-Kung joints subjected to realistic accelerated weathering cycles remains markedly insufficient. Establishing quantitative links between progressive microstructural deterioration and nonlinear mechanical responses [27,28], particularly the attenuation of toughness, is a critical knowledge gap. A significant deficiency exists in physics-based predictive frameworks capable of directly correlating the multidimensional effects of weathering duration and intensity with quantifiable reductions in the structural toughness of Tou-Kung joints.

In the current work, a comprehensive experimental program was undertaken to elucidate the performance degradation of timber Tou-Kung joints subjected to artificial accelerated weathering. By elucidating chemical, microstructural and macroscopic analyses, we systematically quantify how progressive environmental exposure drives multiscale deterioration in these geometrically complex joints. The results establish a clear correlation between weathering duration and nonlinear mechanical behavior, including changes in stiffness and load-bearing capacity. This research provides an indispensable contribution, offering significant value for advancing both scientific conservation practices and engineering approaches related to ancient timber structures.

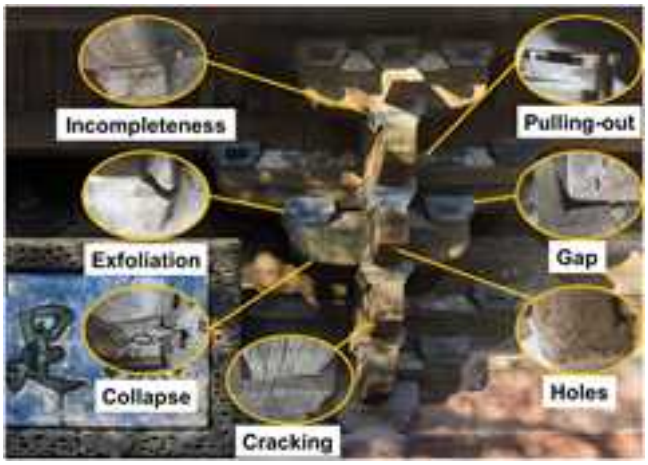

Fig. 1. Types of weathering damage to wooden Tou-Kung joints.

2. Materials and methods

2.1. Specimens configuration

For the assessment of load-bearing capacity in five-stamping Tou-Kung joints within ancient Chinese architecture, twelve 1:10 scale models were constructed regarding the complete Bu-Jian Tou-Kung at Longhu Hall, Yongle Palace in Ruicheng, Shaanxi and the Yingzao Fashi. All component configurations and dimensions were precisely specified per the *Yingzao Fashi*, yielding a five-layer Xia-Ang Tou-Kung with external dimensions of 110 mm in height, 143 mm in width, and 180 mm in length. The Joint configuration is illustrated in Fig. 2. The experimental Tou-Kung joint specimens were fabricated from the Ulmus pumila. This species was selected based on archaeological and architectural evidence indicating its prevalent use in load-bearing components, which served as the geometric prototype for this study [29]. Ulmus pumila exhibits high density, fine and interlocked grain structure, and excellent resistance to splitting, making it historically and mechanically suitable for complex joinery subjected to multi-axial stresses [30].

2.2. The artificial accelerated weathering method

The accelerated weathering process was designed by integrating key provisions from NT Fire053 [31], JSTM J 7001 [32,33], EN 927–6 [34] and ASTM G154:2016 [35]. To simulate the combined effects of solar radiation, cyclic moisture and thermal extremes encountered by historic timber joints in outdoor service environments [2,36,37]. The weathering process configuration is illustrated in Fig. 3. A 24-hour cycle was employed, consisting of 4 h of water spray, 5 h of UV irradiation, 5 h of drying at 60 °C and 10 h of cooling at −20 °C. And the system reliably executed 0–35 cycles of weathering. During spraying, purified water was evenly distributed through nozzles with sample rotation to ensure uniform coverage, under conditions of 16–25℃ ambient temperature and a relative humidity of 70 % or higher. For the UV and drying process, irradiance was set at a level of 1.55 W/(m²·nm), black panel temperature at 60°C and relative humidity between 45 % and 70 %.

The drying temperature of 60 °C aligns with EN 927–6 and reflects measured surface temperatures of sun-exposed wood in temperate climates, which commonly exceed 55 °C [38]. This temperature effectively removes bound water while minimizing desorption-induced gradients that could lead to non-representative cracking [39]. The −20 °C cooling phase follows JSTM J 7001 and ensures complete freezing of free water in wood lumens. It is a dominant mechanism in natural freeze-thaw deterioration [40]. The extended cooling duration provides sufficient time for thermal equilibration and ice nucleation. Prior studies indicate that prolonged subzero exposure has a negligible influence on overall degradation trends when freeze-thaw is fully engaged [41]. Pretreatment in a controlled environment maintained samples for 96 h to stabilize moisture at 20.0 ± 0.5 % before uniaxial compression tests [42]. This approach effectively replicates wood aging, enabling robust assessment of mechanical degradation.

2.2.1. Mass loss measuring

The changes in mass during the weathering process of wooden Tou-Kung joints are affected by several factors, including humidity cycles from water spray, thermal degradation and UV radiation. Among these, the effects of thermal degradation can be quantitatively measured by comparing the mass before and after heat treatment.

After conducting artificial accelerated weathering, the experimental samples were placed in a controlled environment for 96 h until their mass stabilized. Subsequently, four repeated weights were performed using an electronic balance with a precision of 0.01 g, and the average

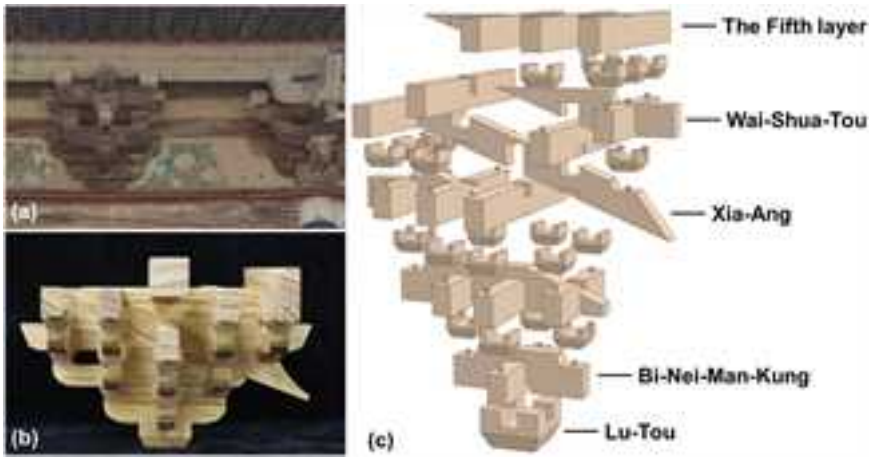

Fig. 2. Structure of the Tou-Kung joints of the Longhu Hall. (a) A physical diagram of Tou-Kung joints, (b) experimental sample diagram and (c) sketch of a Bu-Jian Tou-Kung.

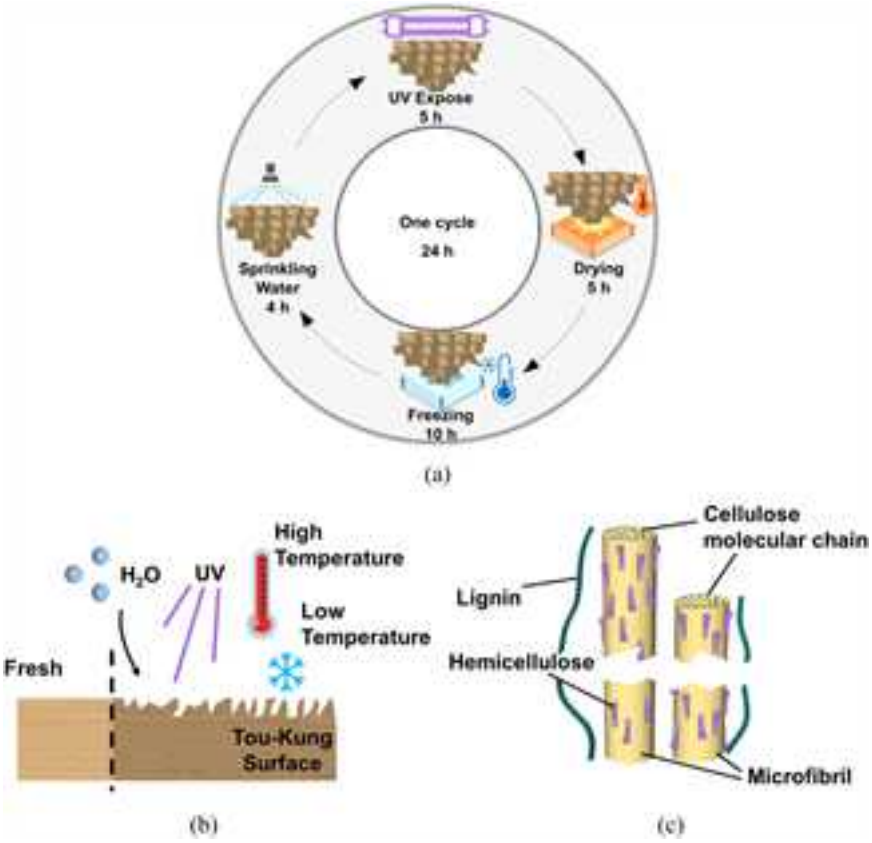

Fig. 3. Artificial accelerated weathering process and sample changes. (a) The illustration of the weathering process configuration, (b) surface changes of weathered wood and (c) microscopic changes of wood after weathering.

mass was calculated. The mass loss rate (*MLR*) was then determined using the formula:

$$MLR = \frac{m_0 - m_i}{m_0} \tag{1}$$

where m_0 is the initial mass of joints; m_i is the mass of the sample after i cycles of weathering; $i = 7, 14, 21, 28, 35$.

2.2.2. *The analysis of surface color RGB*

Utilize the LS 171 handheld colorimeter to capture surface color measurements. Repeat the measurement at a single point three times to ensure that the color value deviation for each measurement of a single sample does not exceed 0.1. This approach helps eliminate the influence of localized color anomalies on the results and enhances the representativeness of the sampling points, as well as the comparability of the data. Select five representative components from top to bottom at the Tou-Kung joints for measurement. For each component, except for the Lu-Tou, measure four points at equal intervals on one side, resulting in a total of eight points. For the Da-Tou component, measure all eight exposed surfaces of its Tou-er. The specific measurement points are illustrated in Fig. 4.

The Lab* three-dimensional colorimetric system, developed by the

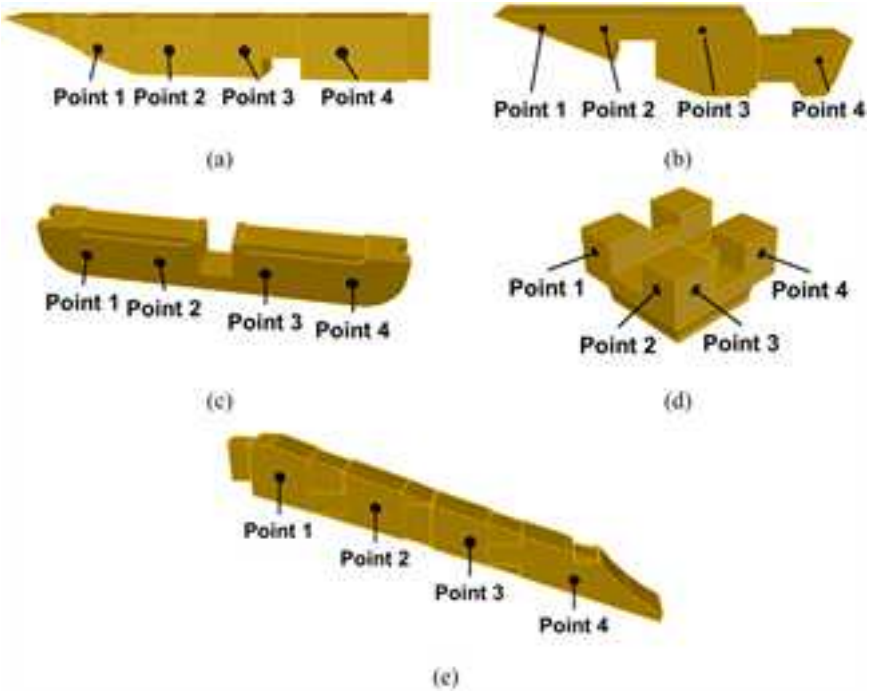

Fig. 4. Measurement point layout. (a) Chen-Fang-Tou, (b) Wai-Shua-Tou, (c) Ni-Dao-Kung, (d) Lu-Tou and (e) Xia-Ang.

International Commission on Illumination (CIE), is employed for color characterization, achieving accurate colorimetric description through quantitation of color perception characteristics. Lightness is represented by the L^* parameter, ranging from 0 to 100 to denote transitions from black to white; the a^* parameter indicates the red-green opponent hue, with negative to positive values signifying shifts from green towards red; and the b^* parameter signifies the yellow-blue opponent hue, with negative to positive values indicating alterations from blue to yellow. Utilizing the color difference calculation approach endorsed by the BS 6923 standard, the color value difference during the weathering of wooden Tou-Kung joints can be expressed as:

$$\Delta E = \sqrt{(L^* - L_0^*)^2 + (a^* - a_0^*)^2 + (b^* - b_0^*)^2} \quad (2)$$

where ΔE is the color difference; L_0^* and L_i^* represent the lightness values of fresh joints and joints weathered for i cycles, respectively; a_0^* and a_i^* correspond to the red-green chromatic values before and after i cycles of weathering; b_0^* and b_i^* denote the yellow-blue chromatic values of fresh and weathered i cycles joints; with $i = 7$, 14, 21, 28 and 35.

2.3. Vertical loading test

To replicate the initiation criteria and progressive crushing behavior of traditional wooden Tou-Kung joints under vertical loading in an indoor setting and to examine the impact of weathering on their load-bearing capacity, an MS-500 nonlinear mechanical test system [43] was utilized. Illustrated in Fig. 5, the system incorporated an image acquisition unit, a servo controller, a mainframe and a hydraulic power supply. Displacement-controlled vertical loading tests were conducted on the Tou-Kung joints. Vertical loading was administered through an electro-hydraulic servo actuator, which simultaneously recorded load and displacement data. A load cell was interfaced between the loading rod and the platen. Considering structural typology, joint configuration and scaling factors, a loading rate of 0.04 mm/s was selected, with the loading point centered on the fifth layer of the Tou-Kung joints. Tests were terminated upon full specimen failure. Load and displacement data were captured in real time with high precision via the servo controller,

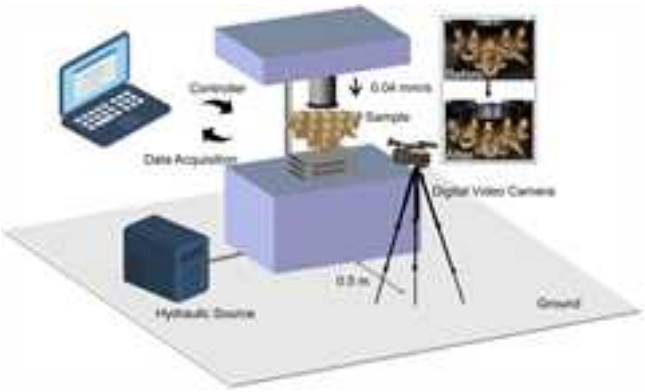

Fig. 5. Vertical load monotone loading test system.

force-displacement transducers, strain amplifiers and data acquisition hardware. The entire testing procedure was documented using a Canon EOS R digital imaging system.

2.4. TGA apparatus

To comparatively investigate the influence of weathering degree on wood composition and its impact on mechanical property variations, thermogravimetric analysis (TGA) was conducted using a NETZSCH TG 209 F3 Tarsus analyzer (NETZSCH-Gerätebau GmbH, Selb, Germany). The measurements were performed in a nitrogen atmosphere (flow rate: 40 mL/min) at a heating rate of 10 °C/min, spanning from 35°C to 800°C. Through real-time recording of the thermogravimetric (TG) curve and subsequent first-order derivative processing, the derivative thermogravimetric (DTG) curve, representing the mass loss rate, was derived. Experimental data were systematically acquired and exported for further derivative processing.

2.5. SEM apparatus

To elucidate microstructural evolution within cellular frameworks during the weathering of Tou-Kung joints in timber structures, observations were conducted using a Hitachi S-4800 field emission scanning electron microscope (FE-SEM; Hitachi High-Tech, Tokyo, Japan), shown in Fig. 6. The experiments used magnification levels of 600 times and 5000 times. Following weathering completion and static equilibration, specimens were sectioned longitudinally to obtain thin slices (3 mm × 5 mm). These slices were secured with conductive adhesive tape, sputter-coated with gold and imaged under secondary electron (SE) mode using an acceleration voltage of 5 kV.

3. Results and discussion

3.1. Weathering effects on the Tou-Kung joints

3.1.1. Mass loss analysis

To assess the impact of artificial accelerated weathering on wooden Tou-Kung joints, mass loss and its rate were quantified across multiple weathering cycles via controlled environmental tests. MLR represents the arithmetic mean of two independently tested specimens per weathering cycle. As shown in Fig. 7, the findings demonstrate a progressive increase in mass loss with the cycling period, particularly after the 21-cycle mark. Concurrently, the mass loss rate exhibits a transient reduction during intermediate stages attributable to water absorption, followed by an escalation caused by component deficiency in later phases, implying that weathering facilitates both transient moisture retention and subsequent structural deterioration.

3.1.2. Color difference analysis

Based on the colorimetric data from Fig. 8, before weathering, the samples exhibited luminosity L^* values ranging from 62 to 69 with a mean of 66.06, a^* values from 7 to 10 with a mean of 8.93 and b^* values from 15 to 23 with a mean of 19.92. As weathering cycles increased and UV irradiation duration was extended, it was found that L^* values progressively decreased, a^* values showed a slight fluctuation increase and b^* values significantly increased, indicating a reduction in wood surface brightness and an enhancement in yellow and red hues. Given the significant positive correlation between color parameters and weathering cycle, the color difference analysis method was utilized to accurately characterize the pattern of surface color changes in the Tou-Kung joint of wooden structures [44].

Fig. 6. SEM apparatus.

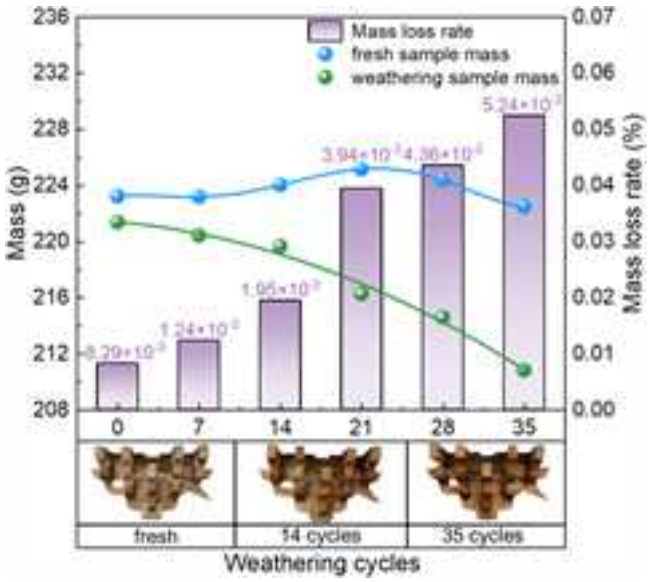

Fig. 7. The mass loss rate of the Tou-Kung joint varies with the weathering cycles.

3.1.3. Thermogravimetric analysis (TGA)

Normalizing the TG curves at 120°C, where physically adsorbed water evaporates and mass stabilizes, accounted for initial weight loss related to moisture. All reported mass losses and residue yields were calculated relative to this normalization baseline, thereby characterizing the intrinsic thermal degradation behavior of wood. Furthermore, to evaluate how wood weathering affects the mechanical performance of Tou-Kung joints and decipher underlying compositional degradation mechanisms, the evolution of constituents was monitored via TG analysis, as shown in Fig. 9. Results demonstrate that extended weathering reduced the mass loss ratio during hemicellulose degradation TG_1 from 27.73 % to 14.10 %, whereas cellulose degradation TG_2 mass loss fluctuated from 61.92 % to 68.35 %. The DTG peak temperature rose progressively from 329.06°C to 363.57°C, while residual carbon rates varied within 13.15 %-22.77 %. All fitted curves achieved coefficients of determination $R^2 \geq 0.98$, collectively demonstrating that weathering preferentially degrades hemicellulose and modifies the relative thermal stability of wood components.

3.1.4. Changes in joint mechanical response

The influence of coupled artificial accelerated weathering, involving alternating high and low temperatures, dry and wet cycles and UV irradiation, on the vertical bearing capacity of timber-structured ancient architectural Tou-Kung joints was examined by applying accelerated weathering treatments for durations of 0–35 cycles. Following weathering, uniaxial compression tests were executed, yielding force-displacement curves for various weathering levels. To precisely identify alterations in the force-displacement response during compression and detect stiffness variations and potential yield points, the raw collected data were subjected to preprocessing. The Savitzky-Golay digital filtering algorithm was employed to smooth the discrete force data, effectively attenuating high-frequency fluctuations attributable to sensor noise or minor mechanical vibrations while preserving the low-frequency trend information of the original dataset maximally. The second derivative was computed numerically for the smoothed force-displacement curve, with displacement designated as the independent variable and the smoothed force as the dependent variable. This derivative represents the instantaneous rate of change in material stiffness during compression. The resultant smoothed second-derivative curve served as a primary metric for feature extraction, enabling quantitative characterization of mechanical behavior transitions under compressive

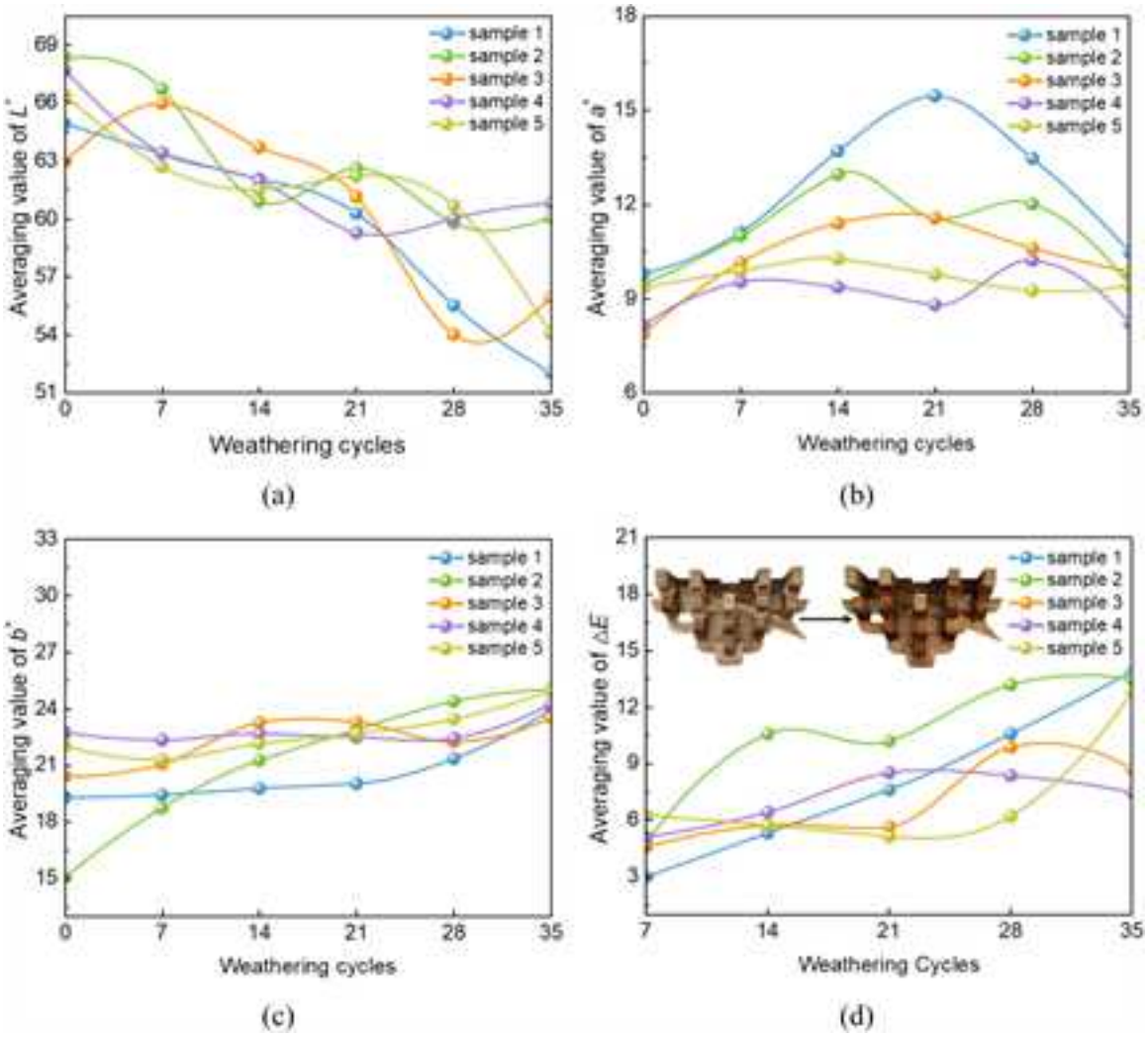

Fig. 8. The CIELAB of the Tou-Kung joint varies with the weathering cycles. (a) Averaging value of L^*, (b) averaging value of a^*, (c) averaging value of b^* and (d) averaging value of $\triangle E$.

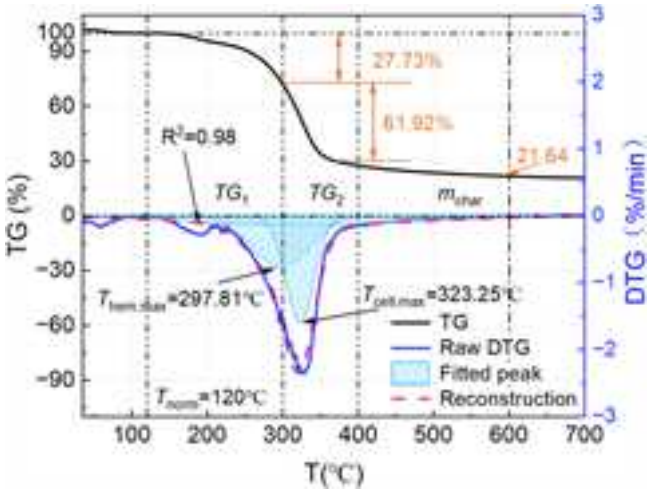

Fig. 9. The stage division of the experimental sample in the combustion process at 10 ℃/min.

loads, such as the shift from the elastic to plastic region.

Fig. 10 shows the vertical pressure-displacement curves of the timber Tou-Kung with different weathering degrees. These curves displayed an initial rise, subsequent decline and final resurgence in load growth rate [45], progressing through eight stages [46]: (I) pre-compaction, (II) elastic, (III) yielding, (IV) load plateau, (V) first strengthening, (VI) second strengthening, (VII) ultimate and (VIII) failure. Critical mechanical parameters are extracted in Table 1. Where k_e denotes the initial stiffness; L_y, L_p, L_r and L_f represent the load-bearing capacities at yield, peak load, ultimate deformation and failure, respectively; while $k_{h,1}$ and $k_{h,2}$ correspond to the stiffnesses during the first and second strengthening stages.

3.1.5. SEM analysis

Macrostructural and microstructural characterization of the surface morphology in six experimental specimens was performed using scanning electron microscopy. Sampling points were selected at the fifth layer within the Tou-Kung joints. Specimen surface textures, vessel lumina diameters and parenchyma cells were comparatively analyzed. Fig. 11 presents the characteristic rupture modulus morphology observed in the specimens.

Wood cell walls consist of the middle lamella, primary wall and secondary wall. Tracheids interconnect via the middle lamella, with cellulose providing skeletal support while hemicellulose and lignin stabilize the internal matrix; lignin additionally preserves middle lamella morphology. Fig. 11(a) illustrates Tou-Kung joints in both fresh

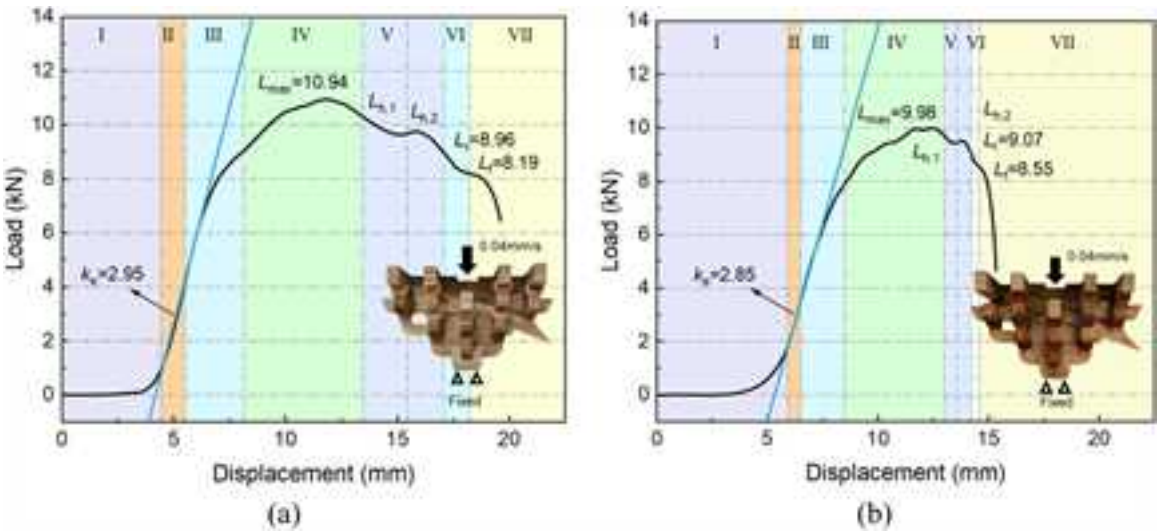

Fig. 10. Vertical pressure-displacement curves of the timber Tou-Kung with different weathering degrees. (a) Fresh sample and (b) weathering 35-cycle sample.

Table 1
Material Parameters of Weathering Tou-Kung Joints.

Weathering cycles	k_e, kN/mm	L_y, kN	L_p, kN	$k_{h,1}$, kN/mm	$k_{h,2}$, kN/mm	L_r, kN	L_f, kN
0	2.95	8.12	10.94	-0.32	-0.43	8.96	8.19
7	3.24	9.11	11.65	-0.60	-0.49	9.92	9.66
14	3.00	8.60	11.77	-0.45	-0.42	9.62	8.87
21	3.13	9.18	11.00	-0.20	0.14	10.71	10.65
28	2.94	9.13	10.40	-0.29	-0.43	8.43	7.79
35	2.85	7.86	9.98	-0.48	-0.58	9.07	8.55

and weathered conditions. The surface morphology of the joints has been significantly damaged due to weathering, accompanied by the presence of decomposition residues. Fig. 11(b) shows fresh samples displaying smooth surfaces, intact tracheid lumens, plump pits, even fractures and microfibrils exhibiting mild surface roughening but no delamination.

Conversely, weathered specimens from Figs. 11(c) to 11(g) exhibited chaotic, degraded surfaces featuring diagonal microcracks and partial cell wall detachment. Microfibril deterioration along tracheid axes disrupted interlayer cohesion, widening pore gaps and loosening fiber bundles. After 21 cycles, microfibrils coarsened and buckled as interfacial bonding weakened. By 28 cycles, cellulose degradation diminished cell wall elasticity, provoking crack propagation through cellulose-rich zones. Concurrent lignin breakdown in the middle lamella reduced intercellular adhesion strength [47]. By 35 cycles, microfibril fragmentation and shedding further compromised structural integrity, inducing surface cracking. These morphological contrasts confirm progressive cellular deterioration and pit expansion due to weathering.

3.2. Effects of weathering on mass loss of Tou-Kung joints

Wood, as a naturally capillary porous material, stores moisture via free water in cell lumens and bound water in cell walls [38], driving mass shifts linked to hygroscopic traits. During early weathering, Tou-Kung joints' mass loss rose from 0.8 % to 1.5 %, with higher initial mass correlating to greater sensitivity, governed by heat-humidity cycle synergy. Cellulose, a hydrolysis-resistant, high molecular weight linear polymer [48], enhances water permeation by increasing surface area. In contrast, hemicellulose, a soluble polysaccharide mixture with short chains and a branched structure [49], degrades easily under heat, moisture, and light, significantly reducing hygroscopic capacity and mass stability [20]. Later, mass loss stabilized at 2.6–3.0 % during a slow-change phase, dominated by water spray washing. UV exposure oxidized lignin, depolymerizing molecules into low-molecular-weight (MW) products and lowering lignin content. Concurrent hemicellulose leaching, extractives and inorganic compounds enlarged porosity and pore size [50], inducing surface powderization and detachment. Temperature-humidity cycles also propagated ray-direction cracks in wood, increasing their length and depth as the wood ages, thereby speeding up weathering. Under these combined mechanisms, samples developed characteristic surface exfoliation and progressive mass loss [51], highlighting multi-faceted erosion mechanisms for timber preservation applications.

3.3. Effects of weathering on the color RGB of Tou-Kung joints

UV radiation is the dominant driver of wood aging, inducing chemical reactions such as lignin oxidation and degradation via photon absorption [52]. As a multiphase composite biomaterial, wood possesses cell walls primarily composed of cellulose fibers, lignin and hemicellulose. Lignin, comprising 20–30 % of the cell wall, is enriched with photosensitive moieties, including aliphatic and aromatic hydroxyl groups. During UV exposure, lignin accounts for 80–95 % of the total UV absorption coefficient, followed by carbohydrates and minor extractives [38]. As the most UV-sensitive cell wall component, lignin not only serves as the primary UV absorber but also transfers energy to cellulose, thereby accelerating its degradation [53]. The depth of light penetration and initiation of photochemical reactions are wavelength-dependent [54]. In artificial accelerated weathering, UV lamps usually emit radiation in the range of 350–400 nm, with a peak at 365 nm, which aligns effectively with the absorption spectrum of lignin. Lignin absorbs UV light significantly starting at 280 nm, peaking around 400 nm. In this range, chromophoric groups like hydroxyl (-OH), carbonyl (C═O), phenolic, and conjugated alkenyl (C═C) absorb photon energy and initiate free-radical chain reactions. Dissociation of molecular bonds produces free radicals, which eventually lead to quinone structures (-C═O-C═O-) through oxidation. Quinone is a secondary chromophore formed through the photodegradation and photooxidation of lignin, which is the primary cause of yellowing and browning of wood surfaces. Consequently, photodegradation exhibits pronounced spatiotemporal heterogeneity. Early-stage aging is dominated by rapid lignin and cellulose oxidation. Following the stabilization of chromophoric groups, degradation propagates toward subsurface regions, coinciding with a plateau in surface discoloration.

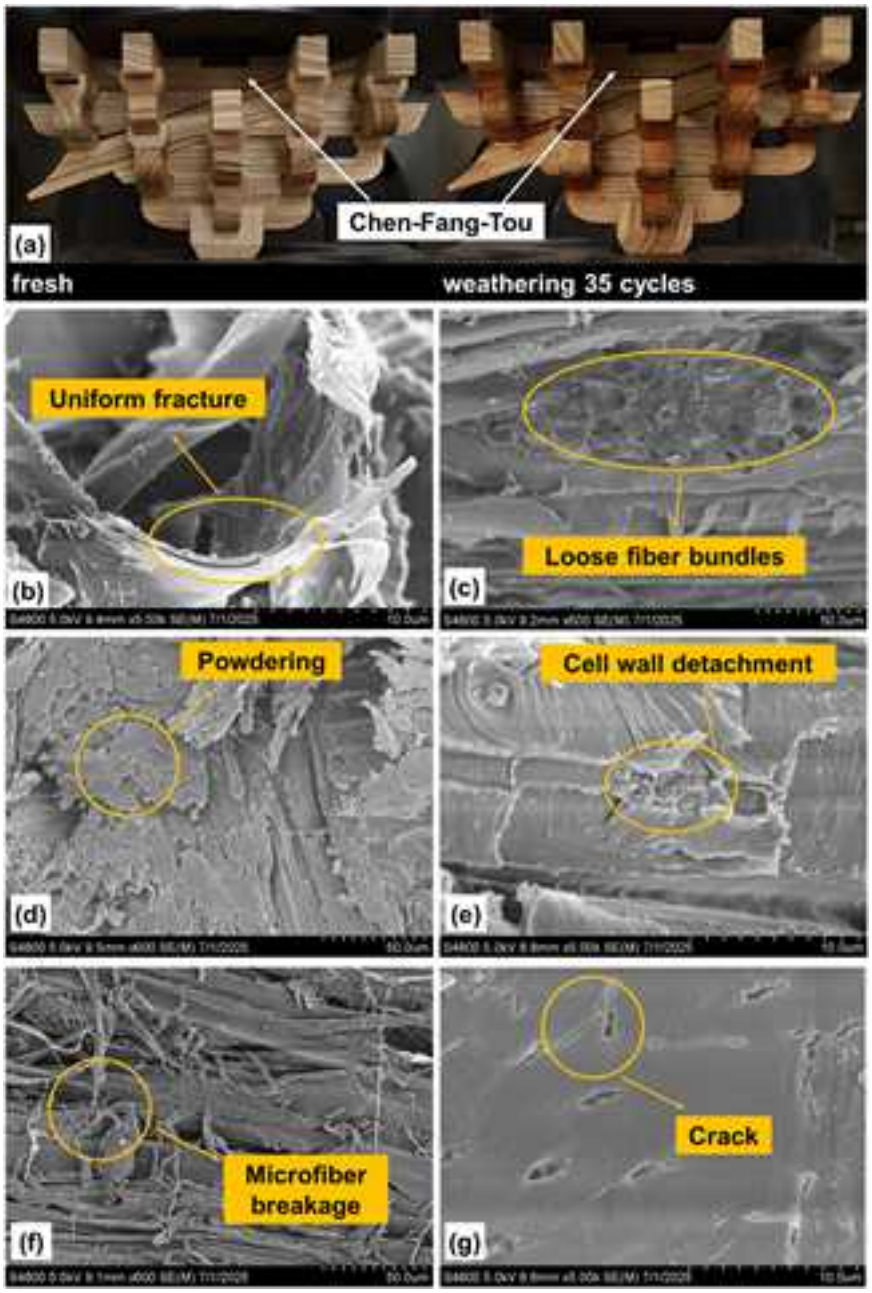

Fig. 11. Scanning electron microscopy (SEM) images showing the microstructural evolution of Tou-Kung joint samples at different weathering cycles. (a) overview of fresh and weathered samples, (b) fresh sample, (c) 7 cycles, (d) 14 cycles, (e) 21 cycles, (f) 28 cycles and (g) 35 cycles.

Alongside photodegradation, concurrent drying, heat treatment, thermal degradation and hydrolysis collectively cause discoloration. As weathering advances, the loss of extractives and leaching of degradation products speed up [55], reducing surface hydrophobicity and increasing wettability. Comparative studies show different responses in dry versus wet aging modes: both experiences decreased lightness L^* and increased redness a^*, yet after 600 h, yellowness b^* in wet samples drops by approximately 50 %, which contrasts sharply with the continuous increase seen in dry samples. Combined with b^* trends, this suggests that during the dry-wet cyclic aging process, the oxidative thermal degradation effect of high-temperature drying has a greater impact on color parameters than the leaching effect of products, dominating the evolution of wood surface color differences.

3.4. Effects of weathering on TG of Tou-Kung joints

The effect of artificial accelerated weathering cycles on the primary chemical constituents of wood was evaluated by calculating the mass fractions of hemicellulose, cellulose, lignin and char via secondary processing of TG data, as shown in Fig. 12. Results indicate that increasing the weathering cycle from 0 to 35 cycles led to a significant decrease in hemicellulose fraction, relatively stable cellulose fraction, minor fluctuations in lignin fraction and a marked increase in char fraction. This suggests accelerated weathering promotes hemicellulose degradation and enhanced char formation. Cyclic hygrothermal exposure degrades hemicellulose and cellulose. Hemicellulose is a heteropolysaccharide with high branching, low polymerization, amorphous structure and short-chain morphology, displaying the poorest thermal stability due to its susceptibility to hydrolysis [56]. Initial mass loss below 250°C was attributed to decomposition of hemicellulose-derived

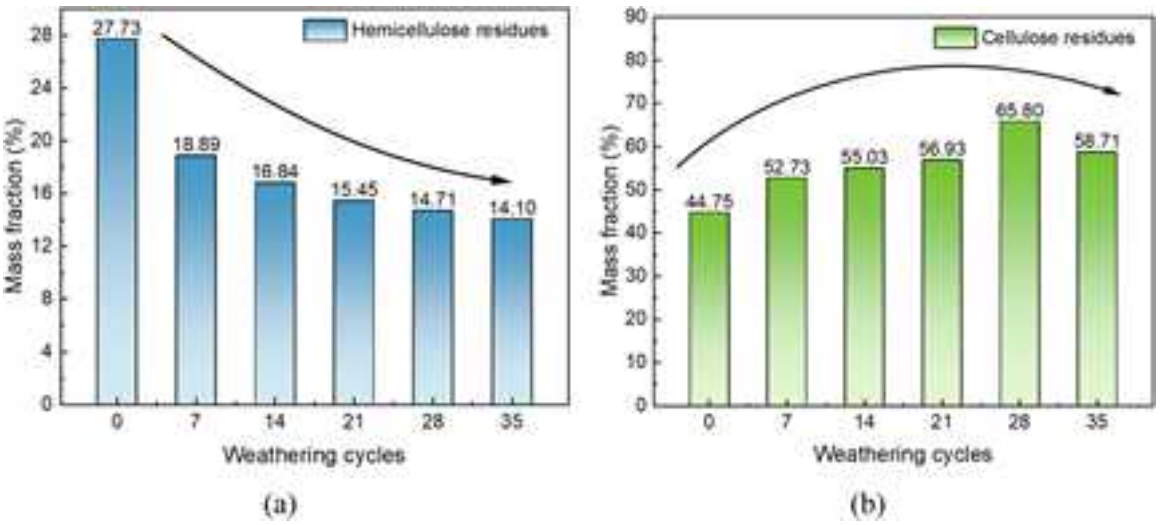

Fig. 12. Mass fractions of hemicellulose and cellulose. (a) Hemicellulose residues and (b) cellulose residues.

acetyl and moisture release [57]. Notably, the DTG curve of aged wood exhibited a 34.51°C peak shift toward higher temperatures and intensified mass-loss rates within 200–250°C relative to fresh wood. These results confirm that accelerated weathering preferentially degraded hemicellulose, thereby increasing cellulose's relative abundance in the wood matrix. Cellulose constitutes a long-chain, highly crystalline polymer formed by interconnected glucose units. Regular molecular packing and an extensive hydrogen-bond network confer exceptional thermal resistance. Strong covalent bonds within molecular chains and intermolecular hydrogen bonding further enable cellulose fibers to withstand high tensile stress [56,58,59]. For weathered wood, the primary cellulose decomposition temperature T_{max} increased from 323.25°C to 359.05°C, accompanied by an approximately 28.30 % increase in peak height and a slight narrowing of the peak shape. These findings demonstrate that cellulose chains recrystallize during weathering.

Owing to its highly cross-linked structure and aromatic rings, lignin demonstrates superior thermal stability. Its decomposition proceeds slowly and continuously over a broad temperature interval, appearing as a broad "tail" on the high-temperature flank of the cellulose peak in DTG curves. As the most UV-sensitive cell wall component, lignin transfers UV radiation to cellulose, provoking its degradation. Char yield predominantly originates from lignin's incomplete pyrolysis products, functioning as a critical indirect indicator of lignin content variation [60]. Moreover, non-monotonic char yield changes arise from competing mechanisms: in intermediate weathering, lignin-hemicellulose complex photolysis boosts carbon retention efficiency [61]. At the critical stage, extended exposure triggers photochemical degradation of surface-proximal lignin, drastically reducing char yield [52]. In later stages, cellulose recrystallization collapses micropores, entrapping pyrolysis volatiles and restoring char yield.

3.5. *Effects of weathering on the mechanical response of Tou-Kung joints*

Initial loading exhibited near-zero load oscillation due to component gaps. After full contact was established, the elastic phase initiated with near-linear load-displacement behavior. Early weathering increased wood hygroscopicity, enhancing elastic stiffness. However, prolonged weathering reduced hygroscopicity and induced component failure, ultimately decreasing stiffness and structural stability. The transition to yielding occurred when the second derivative of the curve exhibited a change from negative to positive, indicating nonlinear displacement growth and a reduced rate under increased load. Moisture absorption during initial weathering improved compressive resistance via swelling, but cellulose and lignin degradation and microfibril fracture [38] weakened joints over time, shortening the yield phase duration. The load plateau began when the second derivative changed sign from positive to negative. Peak load capacity occurred in this phase, reaching 11.77 kN after 14 cycles of weathering before declining to 9.98 kN at 35 cycles. Two consecutive second-derivative sign changes signaled a strengthening onset. Wood embedment theory explains perpendicular-to-grain deformation through direct compression and fiber-stretch interactions, with the latter contributing to strengthening. Accelerated weathering progressively shortened this phase and reduced stiffness through cellulose degradation, microfibril rupture, cell wall collapse, and surface roughness. The defined residual load capacity peaked at 10.71 kN on 21 cycles but remained below initial levels by 35 cycles. The stiffness degradation ratio during the first two strengthening stages is 0.82–0.96 relative to the elastic stage, highlighting that weathering decreases load capacity, stiffness, and accelerates post-peak softening.

To assess the toughness changes of wooden Tou-Kung joints under weathering effects, a dimensionless Toughness Index (*TI*) was developed based on force-displacement data to indicate the level of structural ductility degradation directly.

$$TI = \frac{\delta_{max} - \delta_y}{\delta_r - \delta_y} \tag{3}$$

where δ_{max} is the loading displacement corresponding to the point of maximum vertical bearing capacity; δ_y is the yield displacement corresponding to the yield point; δ_r is the ultimate displacement corresponding to the ultimate point.

As shown in Fig. 13, the *TI* evolved with weathering time: 0.41 at 0 cycles, 0.67 at 7 cycles, 0.46 at 14 cycles, 0.49 at 21 cycles, 0.42 at 28 cycles and 0.70 at 35 cycles. It should be noted that while the *TI* increased at 7 cycles due to moisture-induced plasticization and hygroscopic swelling. And increased at 35 cycles due to loss of structural integrity, rather than intrinsic toughening, a phenomenon also observed in aged polymers and composite biomaterials [62]. For Tou-Kung joints weathered for 35 cycles, structural deficiencies extended the pre-compression phase [63], yielding a larger maximum-load displacement but smaller overall compressive displacement. When excluding structural damage, the toughness index of Tou-Kung joints declined as weathering duration increased. Decreasing *TI* values suggest that the load-bearing displacement converges toward the limit displacement, diminishing load capacity and elevating failure risk. Fig. 13 further reveals a reduction in ultimate displacement at ultimate stress, consistent with the inference that weathering exacerbates mechanical failure at

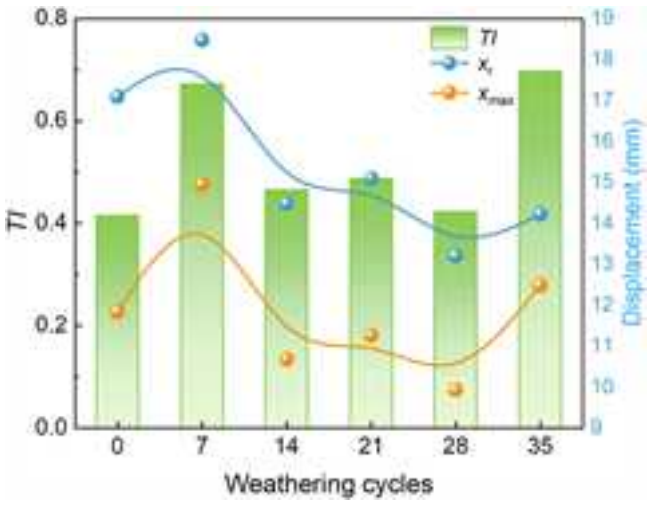

Fig. 13. The *TI* evolved with weathering cycles.

joints.

3.6. Mechanism of Tou-Kung joints degradation

As shown in Fig. 14, the temporal effects of weathering on the mechanical behavior of traditional Tou-Kung joints were investigated through experimental quantification of dynamic load-bearing capacity. During the initial 14-cycle weathering stage, mechanical performance improved significantly, with maximum load capacity reaching 11.77 kN, representing an 8.4 % increase over fresh specimens, driven by moisture-induced material expansion and enhanced compressive resistance. Progressive deterioration subsequently occurred, as evidenced by the reduction in peak load capacity from 11.77 kN to 10.40 kN after 28 cycles, and 9.98 kN after 35 cycles. Nonlinear temporal patterns emerged as time-to-maximum-force decreased to 266.72 s during the 14 cycles before increasing to 245.33 s later. Microstructural analysis demonstrated that early microcrack propagation optimized stress distribution efficiency, while prolonged weathering degraded structural integrity through cellulose chain fracture and hemicellulose dissolution [64]. Observed surface fragmentation and roughening of microfibrils corresponded with failure mode fluctuations arising from local stress concentrations induced by percolating fluids. These findings collectively establish a comprehensive framework for interpreting time-dependent performance degradation in historical

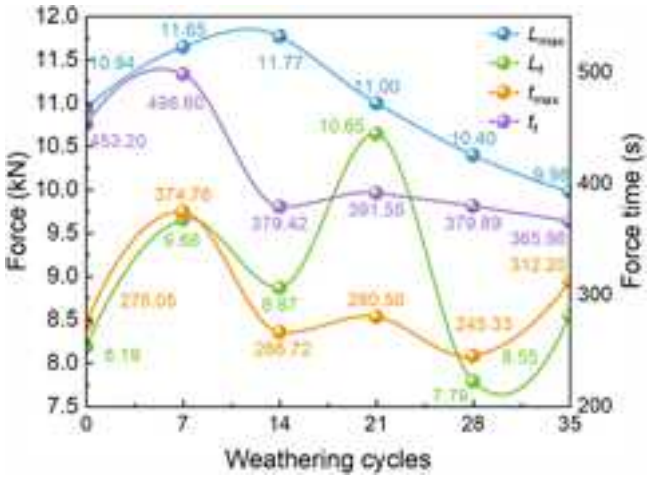

Fig. 14. The maximum bearing capacity, failure bearing capacity and time of wooden Tou-Kung joints change with the degree of weathering.

timber structures.

This study systematically examines the evolution of Tou-Kung joint properties under weathering conditions, focusing on both mechanical performance and microstructural changes, as shown in Fig. 15. Results indicate that Tou-Kung joint undergoes distinct, multi-stage physical and chemical transformations when exposed to weathering, with each stage influencing the mechanical strength and microstructural integrity [65]. As the weathering cycle increases, the hemicellulose mass fraction drops significantly from 27.73 % to 14.10 % and the peak temperature for cellulose thermal decomposition rises from 329.06°C to 363.57°C, indicating molecular chain rearrangement and increased crystallinity [66]. After 21 cycles of weathering, the microfiber surface becomes rough and buckled. By 35 cycles, severe dissociation and fracture along the vessel axis occur, directly related to increased brittleness caused by cellulose recrystallization [67]. The macroscopic mechanical response shows that in the initial weathering stage, hygroscopic expansion briefly raises the peak load by 6.5 %. However, as weathering continues, the peak load decreases at 21 cycles. In the later stage, the peak load drops by 8.8 % compared to the initial value.

In summary, the mechanical properties and microstructural evolution of Tou-Kung joints under weathering conditions are the result of a combination of factors. Hemicellulose hydrolysis initiates a cascade of degradation. Cellulose molecular restructuring, microfibril interfacial weakening and fracture, loss of structural stiffness, and ultimately bearing collapse collectively drive the deterioration of Tou-Kung joints. Through a deeper understanding of these mechanisms, the bearing capacity of Tou-Kung joints can be improved in the future by optimizing the protection technologies, which will provide more reliable technical support for their protection in ancient buildings.

4. Discussion

This study identifies key ways that wood deteriorates. The main processes include breaking down hemicellulose, the photo-oxidation of lignin, the separation of cell walls and the loss of cohesion between layers. These changes happen due to exposure to alternating moisture and heat, as well as UV light. These mechanisms have been observed in a wide range of hardwood and softwood species [18]. The chemical and micromechanical framework from this study may offer insights for assessing the aging of other historic timber types. Degradation rates and extent are influenced by species-specific traits like extractive composition, density, microfibril angle and anatomical heterogeneity [58,68]. While the sequence of damage evolution may be conserved, the time to critical performance thresholds can differ substantially between species.

This study focuses on the Ulmus pumila, a species that has historically been dominant in northern China's official architecture. Therefore, its findings should be understood within this specific context. To apply these results to other types of timber, further validation through comparative aging experiments is necessary. Future research should emphasize multi-species studies to better understand how degradation rates relate to the inherent properties of different materials. This approach will help develop more generalized predictive models for the conservation of heritage timber.

5. Conclusion

This study reveals the cross-scale degradation mechanisms of traditional timber Tou-Kung joints when subjected to environmental stress, utilizing artificial accelerated weathering experiments. These weathering processes trigger a cascade of degradation that impacts both the chemical composition and microstructure of the wood, ultimately leading to a non-linear deterioration of its macroscopic mechanical properties.

(1) Chemical decomposition, particularly the loss of hemicellulose and the oxidation of lignin, directly compromises inter-fibrillar adhesion and reduces the cohesive strength of the wood matrix.

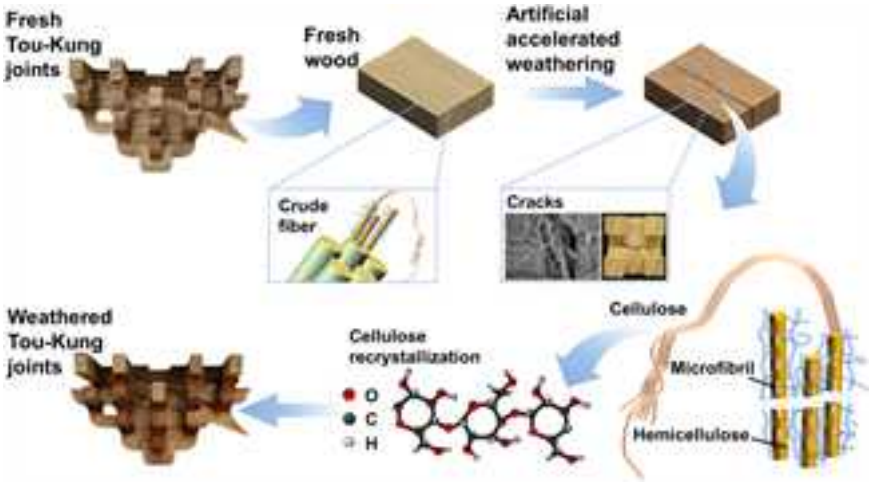

Fig. 15. Schematic diagram illustrating the degradation mechanism of Tou-Kung joints mechanical response at weathering conditions.

(2) Accumulated micro-defects, such as cell wall cracks and ruptured pit membranes, serve as stress concentrators that trigger macroscopic fractures under load.

(3) Concurrent cellulose re-crystallization improves thermal stability but decreases molecular mobility, leading to embrittlement under ambient loading conditions.

(4) Micro-chemical and micro-mechanical changes correlate with key structural indicators, including the decline in peak load capacity and the non-monotonic evolution of the *TI*, as shown in Figs. 8–10.

CRediT authorship contribution statement

Biao Zhou: Writing – review & editing, Project administration, Funding acquisition, Conceptualization. **Shanlong Wang:** Investigation. **Xueting Yang:** Investigation, Data curation. **Wei Li:** Methodology, Formal analysis. **Yoshioka Hideki:** Writing – review & editing, Investigation. **Danping Hao:** Writing – original draft, Visualization, Formal analysis. **Miaomiao Zhao:** Visualization, Investigation. **Kai Wang:** Supervision, Resources, Project administration, Funding acquisition.

Declaration of Competing Interest

The authors declared that they have no conflicts of interest in this work. We declare that we do not have any commercial or associative interest that represents a conflict of interest in connection with the work submitted.

Acknowledgments

This work was supported by the National Natural Science Foundation of China (No.52374248), Beijing Nova Program (No.202504841008), the Ordos Key Research and Development Program (No.YF20240026) , the Fundamental Research Funds for the Central Universities (No.2025ZKPYAQ03) and the Key-Area Research and Development Program of Guangdong Province (No.2024B1111080002).

Data availability

Data will be made available on request.

References

[1] X. Romão, B. Zhou, H. Yoshioka, E. Garbin, Recent contributions addressing the assessment and protection of historic timber structures—VSI Foreword, J. Cult. Herit. 70 (2024) 364–365.
[2] B. Zhou, H. Yoshioka, T. Noguchi, X. Wang, C.C. Lam, Experimental study on fire performance of weathered cedar, Int. J. Archit. Herit. 13 (8) (2019) 1195–1208.
[3] B. Zhou, X. Zhou, M. Chao, Fire protection of historic buildings: a case study of Group-living Yard in Tianjin, J. Cult. Herit. 13 (4) (2012) 389–396.
[4] S. Liang, A pictorial history of Chinese architecture: a study of the development of its structural system and the evolution of its types, MIT Press, Cambridge (Mass.), 1984.
[5] K. Wang, D. Hao, B. Zhou, X. Romão, H. Yoshioka, W. Wang, Z. Wang, Y. Gao, S. Fu, D. Wang, Experimental study on vertical collapse mechanism of Ang structures in historic Chinese wooden buildings, npj Herit. Sci. 13 (1) (2025) 408.
[6] Z. Chen, E. Zhu, F. Lam, J. Pan, Structural performance of Dou-Gong brackets of Yingxian Wood Pagoda under vertical load – An experimental study, Eng. Struct. 80 (2014) 274–288.
[7] J. Wang, X. Cao, H. Liu, A review of the long-term effects of humidity on the mechanical properties of wood and wood-based products, Eur. J. Wood Wood Prod. 79 (2) (2021) 245–259.
[8] M. Borrega, P.P. Kärenlampi, Three mechanisms affecting the mechanical properties of spruce wood dried at high temperatures, J. Wood Sci. 56 (2) (2010) 87–94.
[9] J.Y. Choi, H. Yuk, Y. Choi, J. Nam, S. Kim, Impact of fire-resistant bio-based building materials on fire safety: sustainable retrofit strategies for heritage buildings, Therm. Sci. Eng. Prog. 68 (2025) 104357.
[10] L. Ruggiero, M. Zuena, L. Baroni, L. Valbonetti, S. Ridolfi, M.A. Ricci, A. Sodo, The Minnesang riddle: A multi-analytical approach to an undated colour woodcut, Microchem. J. 174 (2022) 107072.
[11] A.A. Eze, E.R. Sadiku, J.M. Ndambuki, W.K. Kupolati, J. Snyman, I.D. Ibrahim, Aging effects on the physicochemical properties of the wood polymer-based composites, in, in: C. Muthukumar, S.M.K. Thiagamani, S. Krishnasamy, J. Parameswaranpillai, S. Siengchin (Eds.), Biocomposites for Industrial Applications, Woodhead Publishing, 2024, pp. 61–76.
[12] S.K. Hosseinihashemi, A. Rahimi, N. Ayrilmis, Effect of Accelerated Weathering on Color and Physico-mechanical Properties of Wood-plastic Composites with Nano Titanium Dioxide, BioResources 20 (2024) 1200–1213.
[13] K. Imaeda, M. Yamasaki, E. Kojima, C.-G. Lee, T. Sugimoto, Y. Sasaki, Energetic Investigation of Aging Effect on Mechanical Behavior in Wood by Means of XRD Measurement, Int. J. Archit. Herit. 16 (1) (2022) 1–8.
[14] S. Chu, L. Lin, Y. Zhang, D. Wang, Physicochemical structure and micromechanical properties of archaeological wood under alternating dry and wet conditions, Wood Mater. Sci. Eng. 19 (3) (2024) 691–701.
[15] A.K. Matsushita, D. Gonzalez, M. Wang, J. Doan, Y. Qiao, J. McKittrick, Beyond density: Mesostructural features of impact resistant wood, Mater. Today Commun. 22 (2020) 100697.
[16] L. Cheng, J. Dai, Z. Yang, W. Qian, W. Wang, L. Chang, X. Li, Z. Wang, Theoretical and experimental research on moisture content and wood property indexes based on nondestructive testing, BioResources 15 (1) (2020) 1600–1616.
[17] W. Zhong, Z. Zhang, X. Chen, Q. Wei, G. Chen, X. Huang, Multi-scale finite element simulation on large deformation behavior of wood under axial and transverse compression conditions, Acta Mech. Sin. 37 (7) (2021).
[18] J. Song, J. Zhao, J. Deng, S. Lu, G. Hang, Y. Zhang, C.-M. Shu, Effect mechanism of dry and wet alternate ageing on wood during exothermic behaviour, J. Therm. Anal. Calorim. 149 (18) (2024) 10277–10295.
[19] B. Jelle, Accelerated climate ageing of building materials, components and structures in the laboratory, J. Mater. Sci. 47 (18) (2012) 6475–6496.
[20] R. Herrera, A. Arrese, P.L. de Hoyos-Martinez, J. Labidi, R. Llano-Ponte, Evolution of thermally modified wood properties exposed to natural and artificial weathering and its potential as an element for façades systems, Constr. Build. Mater. 172 (2018) 233–242.
[21] K. de la Caba, P. Guerrero, M. del Rio, I. Mondragon, Weathering behaviour of wood-faced construction materials, Constr. Build. Mater. 21 (6) (2007) 1288–1294.
[22] S.-F. Tung, H.-C. Su, C.-T. Tzeng, C.-M. Lai, Experimental and Numerical Investigation of a Room Fire in a Wooden-Frame Historical Building, Int. J. Archit. Herit. 14 (1) (2020) 106–118.

[23] Y. Lin, Q. Chun, W. Zhao, C. Zhang, Q. Chen, Q. Hua, Research on the simplified model for early Chinese Dou-gong under horizontal load, Structures 74 (2025) 108570.
[24] K. Liu, Q. Yang, P. Yu, The Analytical Model and Horizontal Resistance of the Column-Head Dou-Gong in the Traditional Chinese Timber Structure, Int. J. Archit. Herit. 19 (7) (2025) 1181–1199.
[25] C. Wu, J. Xue, D. Song, G. Ren, J. Zhang, Mechanical performance of inclined Dougong bracket sets under vertical load: experimental tests and finite element calculation, J. Build. Eng. 45 (2022) 103555.
[26] E. Sesana, A.S. Gagnon, C. Ciantelli, J. Cassar, J.J. Hughes, Climate change impacts on cultural heritage: a literature review, WIREs Clim. Change 12 (4) (2021) e710.
[27] C. Zhang, Q. Chun, Y. Lin, H. Wang, P. Li, Experimental and nonlinear finite-element analysis study on lateral push resistance of San-dou components perpendicular and parallel to grain in traditional timber buildings, J. Wood Sci. 68 (1) (2022) 41.
[28] X. Wang, L. Zhao, B. Xu, Y. Li, S. Wang, Y. Deng, Effects of accelerated aging treatment on the microstructure and mechanics of wood-resin interphase, Holzforschung 72 (3) (2018) 235–241.
[29] L. Han, K. Wang, W. Wang, J. Guo, H. Zhou, Nanomechanical and topochemical changes in elm wood from ancient timber constructions in relation to natural aging, Materials (2019) 786.
[30] Y. Chen, W. Guo, Mechanical properties evaluation of two wood species of ancient timber structure with nondestructive testing methods, BioResources 11 (3) (2016) 6600-6612.
[31] 2003, NT Fire 053 Nordtest Method. Accelerated weathering of fire-retardant-treated wood for fire testing.
[32] M. Nakamura, H. Yoshioka, M. Kanematsu, T. Noguchi, S. Hagihara, A. Yamaguchi, K. Shimizu, T. Sugita, Y. Matsumoto, Y. Nishio, T. Hayakawa, Reaction-to-fire performance of fire-retardant treated wooden facades in Japan with respect to accelerated weathering, MATEC Web Conf. 46 (2016) 05011.
[33] JSTM J 7001, Test. Method Therm. Deform. Durab. Real. Scale Exter. wall (1996).
[34] Paints and varnishes, Coating materials and coating systems for exterior wood - Part 6: Exposure of wood coatings to artificial weathering using fluorescent UV lamps and water, CEN (2006), 21P.;A4.
[35] 2016, Standard Practice for Operating Fluorescent Ultraviolet (UV) Lamp Apparatus for Exposure of Nonmetallic Materials.
[36] K. Wang, D. Hao, X. Wang, C. Jiang, Y. Hideki, M. Ge, X. Wang, B. Zhou, Experimental study of combustion and upward flame spread characteristics of accelerated weathered pine, Int. J. Archit. Herit. (2025) 1–19.
[37] M. Long, L. Yi, L. Yan, Z. Xu, J. Zheng, Comparative analysis of microstructure, combustion characteristics and mechanical properties of Pinus massoniana lamb. under natural aging conditions, Therm. Sci. Eng. Prog. 48 (2024) 102425.
[38] K. Kránitz, W. Sonderegger, C.-T. Bues, P. Niemz, Effects of aging on wood: a literature review, Wood Sci. Technol. 50 (1) (2016) 7–22.
[39] A.A. Chiniforush, A. Akbarnezhad, H. Valipour, S. Malekmohammadi, Moisture and temperature induced swelling/shrinkage of softwood and hardwood glulam and LVL: an experimental study, Constr. Build. Mater. 207 (2019) 70–83.
[40] K. Charra-Vaskou, E. Badel, G. Charrier, A. Ponomarenko, M. Bonhomme, L. Foucat, S. Mayr, T. Améglio, Cavitation and water fluxes driven by ice water potential in Juglans regia during freeze–thaw cycles, J. Exp. Bot. 67 (3) (2015) 739–750.
[41] J.D. McNatt, C.L. Link, Analysis of ASTM D 1037 accelerated-aging test, Prod. J. 39 (10) (1989) 51–57.
[42] B. Zhou, K. Wang, Y. Liuchen, Y. Li, X. Sun, F. Zhu, W. Ke, X. Wang, B. Qiu, Y. Han, Experimental study of upward flame spread over discrete weathered wood chips, Int. J. Archit. Herit. 16 (12) (2022) 1797–1808.
[43] M. He, D. Liu, W. Gong, C. Wang, J. Kong, S. Du, S. Zhang, Development of a testing system for impact rockbursts, Chin. J. Rock. Mech. Eng. 33 (09) (2014) 1729–1739.
[44] W. Ke, W. Yang, B. Zhou, K. Wang, J. Sun, X. Sun, M. Xu, Q. Chen, B. Qiu, W. Wang, X. Wang, The color change analysis of historic wooden remains after fire-suppression by fluorinated chemical gases, Herit. Sci. 9 (1) (2021) 93.
[45] X. Dong, L. Ma, J. Xue, Mechanical behaviors of Tou-Kung in historic timber structures subjected to vertical load, Structures 47 (2023) 1352–1365.
[46] M. Dorn, K. de Borst, J. Eberhardsteiner, Experiments on dowel-type timber connections, Eng. Struct. 47 (2013) 67–80.
[47] Y. Ouadou, D. Aliouche, M.-F. Thevenon, M. Djillali, Characterization and photodegradation mechanism of three Algerian wood species, J. Wood Sci. 63 (3) (2017) 288–294.
[48] J.I. Hedges, The Chemistry of Archaeological Wood. Archaeological Wood, American Chemical Society, 1989, pp. 111–140.
[49] M. Åkerholm, L. Salmén, Interactions between wood polymers studied by dynamic FT-IR spectroscopy, Polymer 42 (3) (2001) 963–969.
[50] K. Kránitz, 2014, Effect of natural aging on wood.
[51] M. Žlahtič Zupanc, Influence of artificial and natural weathering on the moisture dynamic of wood, Bioresources 12 (2016) 117–142.
[52] M. Kropat, M. Hubbe, P. Laleicke, Natural, accelerated, and simulated weathering of wood: A Review, Bioresources 15 (2020) 9998–10062.
[53] M.-l Kuo, N. Hu, Ultrastructural changes of photodegradation of wood surfaces exposed to UV, Holzforschung 45 (5) (1991) 347–353.
[54] Y. Kataoka, M. Kiguchi, R.S. Williams, P.D. Evans, Violet light causes photodegradation of wood beyond the zone affected by ultraviolet radiation, Holzforschung 61 (1) (2007) 23–27.
[55] D. Fengel, Aging and fossilization of wood and its components, Wood Sci. Technol. 25 (3) (1991) 153–177.
[56] H. Yang, R. Yan, H. Chen, D.H. Lee, C. Zheng, Characteristics of hemicellulose, cellulose and lignin pyrolysis, Fuel 86 (12) (2007) 1781–1788.
[57] H. Yang, R. Yan, H. Chen, C. Zheng, D.H. Lee, D.T. Liang, In-depth investigation of biomass pyrolysis based on three major components: hemicellulose, cellulose and lignin, Energy Fuels 20 (1) (2006) 388–393.
[58] M. Poletto, A.J. Zattera, R.M.C. Santana, Thermal decomposition of wood: Kinetics and degradation mechanisms, Bioresour. Technol. 126 (2012) 7–12.
[59] V. Mamleev, S. Bourbigot, M.Le Bras, J. Yvon, The facts and hypotheses relating to the phenomenological model of cellulose pyrolysis: interdependence of the steps, J. Anal. Appl. Pyrolysis 84 (1) (2009) 1–17.
[60] J. Yun, Q. Yang, G. Liu, Mechanisms of lignin degradation and persistent free radical formation under light or thermal exposure, Cell Rep. Sustain. 2 (1) (2025) 100267.
[61] Y. Zhao, U. Shakeel, M. Saif Ur Rehman, H. Li, X. Xu, J. Xu, Lignin-carbohydrate complexes (LCCs) and its role in biorefinery, J. Clean. Prod. 253 (2020) 120076.
[62] P. Niemz, W. Sonderegger, P.J. Gustafsson, B. Kasal, T. Polocoşer, Strength Properties of Wood and Wood-Based Materials, in: P. Niemz, A. Teischinger, D. Sandberg (Eds.), Springer Handbook of Wood Science and Technology, Springer International Publishing, Cham, 2023, pp. 441–505.
[63] M. Britch, N. Gorbachov, I. Koznacheev, D. Makarenko, Elastic tensions in a wood material subjected to thermo-mechanical treatment by pressure drop, Therm. Sci. Eng. Prog. 16 (2020) 100457.
[64] A. Ghavidel, A. Scheglov, V. Karius, C. Mai, A. Tarmian, W. Vioel, V. Vasilache, I. Sandu, In-depth studies on the modifying effects of natural ageing on the chemical structure of European spruce (Picea abies) and silver fir (Abies alba) woods, J. Wood Sci. 66 (1) (2020) 77.
[65] V.Bd.M. Aquino, M.S. Bertolini, C.A.Gd Morais, T.H. Almeida, D.H. Almeida, F.A. R. Lahr, A.L. Christoforo, Effect of artificial weathering on physical and mechanical properties of wood, Rev. Árvore 45 (2021).
[66] C.A. Beuthe, M.R. Foruzanmehr, M. Riahinezhad, E. Esmizadeh, P. Collins, I. Lopez-Carreon, Effects of hydrolytic and freeze-thaw aging on the performance of spruce wood, Eur. J. Wood Wood Prod. 83 (2) (2025) 76.
[67] D. Kačíková, A. Eštoková, M. Gaff, E. Kmeťová, J. Kúdela, F. Kačík, Thermal analysis of thermally treated spruce wood after its accelerated aging, J. Therm. Anal. Calorim. 150 (5) (2025) 3283–3295.
[68] S.S. Arpaci, E.D. Tomak, M.A. Ermeydan, I. Yildirim, Natural weathering of sixteen wood species: Changes on surface properties, Polym. Degrad. Stab. 183 (2021) 109415.